

Author's Accepted Manuscript

Influence on present-day coastal dynamics and evolution of a relict subaqueous delta lobe: Sol de Riu lobe, Ebro Delta

Caroline Lavoie, José A. Jiménez, Miquel Canals, Galderic Lastras, Ben De Mol, David Amblas, Camino Liqueste, Marc De Batist, John E. Hughes Clarke



www.elsevier.com/locate/csr

PII: S0278-4343(13)00392-0
DOI: <http://dx.doi.org/10.1016/j.csr.2013.11.021>
Reference: CSR2927

To appear in: *Continental Shelf Research*

Received date: 3 April 2013
Revised date: 10 November 2013
Accepted date: 20 November 2013

Cite this article as: Caroline Lavoie, José A. Jiménez, Miquel Canals, Galderic Lastras, Ben De Mol, David Amblas, Camino Liqueste, Marc De Batist, John E. Hughes Clarke, Influence on present-day coastal dynamics and evolution of a relict subaqueous delta lobe: Sol de Riu lobe, Ebro Delta, *Continental Shelf Research*, <http://dx.doi.org/10.1016/j.csr.2013.11.021>

This is a PDF file of an unedited manuscript that has been accepted for publication. As a service to our customers we are providing this early version of the manuscript. The manuscript will undergo copyediting, typesetting, and review of the resulting galley proof before it is published in its final citable form. Please note that during the production process errors may be discovered which could affect the content, and all legal disclaimers that apply to the journal pertain.

Influence on present-day coastal dynamics and evolution of a relict subaqueous delta lobe: Sol de Riu lobe, Ebro Delta

Caroline Lavoie^{a1,2}, José A. Jiménez^b, Miquel Canals^{a*}, Galderic Lastras^a, Ben De Mol^c, David Amblas^a, Camino Liqueste^a, Marc De Batist^d, John E. Hughes Clarke^e

^aGRC Geociències Marines, Departament d'Estratigrafia, Paleontologia i Geociències Marines, Facultat de Geologia, Universitat de Barcelona - C/Martí i Franquès s/n - Campus de Pedralbes, Barcelona, 08028, Spain.

^bLaboratori d'Enginyeria Marítima, ETSECCPB, Universitat Politècnica de Catalunya, BarcelonaTech, C/ Jordi Girona 1-3, Campus Nord ed. D1, Barcelona, 08034, Spain.

^cGRC Geociències Marines, Parc Científic de Barcelona, Campus Diagonal, Barcelona, 08028, Spain.

^dRenard Centre of Marine Geology, Dept. of Geology and Soil Science, Geological Institute, Ghent University, Krijgslaan 281 s. 8, Gent, B-9000, Belgium.

^eOcean Mapping Group, Dept. Geodesy and Geomatics Engineering, University of New Brunswick, Fredericton (NB), E3B 5A3, Canada.

*Corresponding author: Tel.: +34 93 402 1369; fax: +34 93 402 1340.

E-mail address: clavoie@ua.pt

E-mail: clavoieblais@hotmail.com

E-mail address: miquelcanals@ub.edu

Abstract

We use high-resolution swath-bathymetry data to characterise the morphology of the abandoned subaqueous Sol de Riu delta lobe in the Ebro Delta, Western Mediterranean Sea. This study aims to assess the influence of the delta lobe on present-day coastal dynamics in a micro-tidal environment. Detailed mapping of the relict Sol de Riu lobe revealed set of bedforms interpreted as footprints of human activities: seasonal V-shaped bedforms on the middle shoreface due to boat anchoring and trawking marks of few decades old between 16 and 18 m

¹ Present address: Departamento de Geociências, Universidade de Aveiro - Campus Universitário de Santiago, Aveiro, 3810-052, Portugal.

² Tel.: +351 918 778 853.

water depth. Estimations of the mobility of bottom sediment showed that the shallowest shoreface (i.e. water depths below 7 m) is the most dynamic part of the relict lobe, while the middle shoreface displays significant changes in bottom morphology. The deepest shoreface (i.e. water depths in excess of 15 m), which corresponds to the front of the lobe, is defined by a very small potential for morphological change. Wave propagation simulations showed that the typical wave climate in the study area, which is dominated by short-period waves of 4 s, is not significantly affected by the presence of the relict lobe. On the other hand, the relict lobe affects the most energetic wave conditions ($T_p \geq 7$ s) acting as a shoal that results in the concentration of wave energy in the northwestern part of the lobe. The relict lobe along the northern hemidelta coast influences wave-induced littoral sediment dynamics as it modifies the wave propagation pattern with respect to a situation without the lobe.

Highlights

- We use high-resolution swath-bathymetry data and Seismic profiles.
- We interpret bedforms as footprints of human activities.
- Estimations of the mobility of bottom sediment.
- Down to 15 m water depth the relict lobe is active and eroding.
- Sol de Riu relict lobe played a very significant role in the morphological evolution.

Keywords

Multibeam bathymetry, seismic reflection profiling, seafloor morphology, coastal sediment dynamics, anthropogenic activities, gas-charged sediment

1. Introduction

Coastal erosion is a major worldwide problem especially for developed shorelines. Low-lying coasts in general and deltas in particular are among the most affected coastal environments due to natural reasons but, more importantly, to human influence. After several centuries of growth, the seaward development of the Ebro Delta, along the NW Mediterranean coastline of Spain, changed a few decades ago mainly as a response to the decrease in riverine sediment supply due to river damming (e.g. Jiménez and Sánchez-Arcilla, 1993; Lique et al., 2004; Maldonado, 1972, 1975, 1986; Palanques et al., 1990; Varela et al., 1986). Studies on the vulnerability of the deltaic system concluded that its modern evolution is mainly driven by agents inducing coastal 'reshaping' (Jiménez and Sánchez-Arcilla, 1993; Jiménez et al., 1997a, b, 2012; Sánchez-Arcilla et al., 1993, 1996; Valdemoro et al., 2007). The coastal response showed both highly vulnerable sediment-depleted stretches and areas that are experiencing sediment accretion. Overall, those studies illustrate the recent disequilibrium of the system at different timescales under a general frame of intensifying socio-economic stresses and conflicts, as the Ebro Delta sustains a valuable ecosystem with high environmental, fishing and tourist values, in addition to an intensive agricultural use mainly for rice production. Of the 320 km² of the subaerial Ebro Delta, 20 % are natural areas, 75 % is arable land (of which 83 % are rice fields) and 5 % is urbanised, for a total of about 50,000 inhabitants.

The evolution of the Ebro Delta during the Holocene has been investigated by several authors (e.g. Díaz et al., 1990; Maldonado, 1972; Maldonado and Riba, 1971; Somoza et al., 1998) who illustrated a seaward outbuilding of the delta by successive lobes, later abandoned and partially eroded. Maldonado and Riba (1971) and Maldonado (1972, 1986) were the earliest authors to evidence four abandoned subaqueous deltaic lobes built out following the most recent migrations of the Ebro River lower courses (Fig. 1A). One of these lobes is known as the Sol de Riu lobe,

which was active between the 14th and 18th centuries (Maldonado, 1986; Somoza et al., 1998). The Sol de Riu lobe is located in front of La Marquesa sandy beach in the northern hemidelta coast. This sandy stretch presents a uniform rectilinear shoreline and its width varies depending on the shoreward limit of different rice paddies located inshore (Fig. 1B, C). As a general trend, La Marquesa beach has been retreating since the second half of the 20th century and its narrowest parts are frequently breached and overwashed during large storms leading the inundation of the hinterland by salty water (Jiménez et al., 2012). Due to these erosion problems, a protection project has been launched by the Spanish government to protect La Marquesa beach. The project consists in recovering a 500 m wide land strip landwards of the present beach to create a buffer zone to facilitate accommodation space for the beach.

Until now, the offshore morphological data of the Ebro Delta was mainly based on single beam echosoundings, published as interpolated contour maps that provided a coarse overview of the morphology, and offshore seismic reflection profiles. In this paper, high-resolution swath-bathymetry and inshore seismic reflection data are used to enlarge previous knowledge on the subaqueous part of the Ebro Delta. Here we analyse in particular and for the first time the detailed morphology of the relict Sol de Riu lobe located in front of La Marquesa beach, and assess its role in controlling present-day coastal dynamics. This study is both of general and local significance, as it illustrates the role of relict deltaic lobes on modern coastal sediment dynamics and helps to better understand the evolution of La Marquesa beach and the likely consequences of present and future restoration actions.

Fig. 1

2. Study area

The Ebro Delta is located about 200 km southwest of Barcelona (NW Mediterranean coast, Fig. 1), in the province of Tarragona, occupying a total surface of about 800 km² including the subaerial and subaqueous (480 km²) parts. The delta has a 50 km long sandy coastline, of which the main modern features are a central lobe (Cap Tortosa) that is flanked to the north and south by two spits (El Fangar and La Banya). Particularly prominent is the 6.5 km long El Trabucador narrow sandy barrier connecting La Banya spit with the main deltaic body (Fig. 1A). About half of the deltaic plain is less than 0.5 m above the mean water level, which makes the Ebro Delta particularly vulnerable to flooding (Alvarado-Aguilar et al., 2012). Along the shoreface various relict deltaic lobes have been identified indicating former Ebro river mouth positions. Among them is the northeasternmost Sol de Riu lobe, which is our study target (Fig. 1A).

2.1 Oceanographic regime

The study area is a micro-tidal environment with an astronomical tidal range of about 25 cm. However, change in water level caused by local meteorological conditions are frequent in the area reaching values up to 50 cm under the influence of low pressure centres passing along the Catalan coast. Previous studies showed that waves are the most important forcing agent in the Ebro Delta to mobilize and transport coastal sediments and, thus, to control sediment dynamics and seafloor changes on the inner shelf and shoreline (Jiménez et al., 1997a, 1999, 2002; Palanques et al., 2002).

Wave climate is characterised by a yearly average wave height (H_s) of about 0.8 m and a mean peak period (T_p) of about 4 s, which is consistent with an associated restricted fetch (Bolaños and Sánchez-Arcilla, 2006; García et al., 1993; Jiménez et al., 1997a). From the directional standpoint, three main wave components are present in the area (E, S and NW) where

the eastern waves being the dominant ones in terms of energy and, thus, control the littoral dynamics (Fig. 2) (Jiménez and Sánchez-Arcilla, 1993; Jiménez et al., 1997a). The wind-induced currents play a relevant role on the transport of fine sediment re-suspended from the shoreface (Guillén et al., 2002; Jiménez et al., 1999) and discharged by the Ebro River (Durand et al., 2002).

Fig. 2

3. Methods

3.1 Morphological and geophysical data

The Sol de Riu lobe was swath-mapped in summer 2004 using a 300 kHz Kongsberg EM3000 dual echosounder system to characterize the seafloor, both from a quantitative and qualitative point of view. The dual transducer heads were externally mounted at the bow of the *Arraix* survey boat as part of the EU funded PRODELTA RTD project. Multibeam raw data were ping edited to remove false soundings using CARIS HIPS software. Corrections for variations in sound velocity and water level were applied. The assigned water level correction for the study area concerns both astronomical tide (~25 cm maximum amplitude) and residual effects (local meteorological conditions and water density variation) from the nearest gauging station located at L'Ampolla (Fig. 1A). The swath-bathymetry imagery is gridded at a cell size of 1 m and starts at water depths larger than 9 m.

Semi-quantitative seafloor acoustic backscatter data were extracted from multibeam data and a mosaic representing the intensity of sound backscattered from the seafloor was generated. The multibeam backscatter imagery refers to decibel backscatter strength (dB) where the scale values range between -128 and 0. The composite backscatter image is used to constrain the spatial distribution of the sediment in the study area, assuming that the sediment grain size distribution is

the main factor influencing the amount of acoustic energy backscattered by the seafloor since 1) it relates both to surface roughness and volumetric heterogeneity (e.g. Goff et al., 2000) and 2) the study area is characterized by a gentle slope gradient, without any major topographic irregularity. A similar approach was tested and applied in the nearby Llobregat prodelta to the north (Liquete et al., 2010). Fourteen bottom sediment samples taken with a Van Veen grab sampler were used to groundtruth the backscatter imagery (Fig.1A). In addition, three summer beach system profiles extending from the shoreline down to 15 m depth were obtained across the central part of the Sol de Riu lobe (named SRL, 5.8 km long), at its northern limit (INT, 4.5 km long), and outside (FAN, 1.8 km long) (Fig. 1A). The beach system profiles were obtained by single beam bathymetric surveying.

High-resolution single channel seismic reflection profiles (Fig. 1A) were also collected onboard the *Arraix* in 2004 using a 200 J Seistec boomer with a sampling frequency of 32 kHz. The data were processed with a band pass frequency filter of 500 - 3000 Hz, a swell filter, a spiking deconvolution and a centered Automatic Gain Control of 200 ms. Their horizontal resolution is ~3 m and the vertical one is ~0.5 m. The swath-bathymetry data were used as the baseline to shift the seismic profiles by matching the digitized seafloor from the seismic profiles to the bathymetry.

3.2 Bottom sediment transport

The mobility of bottom sediment on the inner shelf of the Ebro Delta was estimated in water depths ranging from 7.5 m, in the middle shoreface, to 40 m. To do this, first, we gathered the sediment grain size from previous studies such as those reported by Díaz et al. (1996) and Guillén and Palanques (1997). These authors found a typical seaward fining sequence which is locally interrupted where relict deltaic lobes appear. In general, the average sand-clay transition depth (h_{SMT}), where the dominant grain size changes from sand to silt and clay, is identified at about 12 m water depth (Guillén and Jiménez, 2009). However, this depth limit varies along the

delta, with deepest values (~18 m) close to the position of relict deltaic lobes as it is the case of the Sol de Riu lobe (Guillén and Palanques, 1997). According to existing data, the sand fraction of the bottom sediment below 7 m depth is constrained between 0.125 mm and 0.063 mm, with the latter value corresponding to the sediment fraction commonly used to define the position of h_{SMT} in continental shelves (Dunbar and Barrett, 2005; George and Hill, 2008).

The required conditions to mobilize these fine sands at the bottom were estimated by assuming the Shields criterion to be valid (Madsen and Grant, 1976). These conditions were calculated by using the analytical expression of Soulsby and Whitehouse (1997), which predicts that the critical bottom shear stresses (τ_{cr}) required to mobilize sediment with a diameter of 0.125 mm and 0.063 mm are $0.106 \text{ N}\cdot\text{m}^{-2}$ and $0.133 \text{ N}\cdot\text{m}^{-2}$, respectively (Guillén and Jiménez, 2009). It has to be considered that although the Shields criterion is not applicable to sediments in the mud-silt range due to the presence of cohesion forces, resuspension of fine sediments is also related to the maximum shear stress at the bottom (e.g. Maa et al., 1998; Wolanski et al., 2005).

Previous experimental studies in the Ebro delta inner shelf permit to characterize the system in terms of bottom sediment mobility. Thus, the remobilization of the sediment in the inner shelf presents a pulsating behaviour, being largely controlled by the presence of storm events (Jiménez et al. 1999; Palanques et al. 2002). The resuspension of sediments in the inner shelf is primarily produced by wave-induced bottom shear stress during storms (about one-third of the time) and in secondary importance by wind-induced currents (occurring very sporadically) (Palanques et al., 2002). Thus, the main role of currents is to advect the sediment mobilized from the bottom inducing a dominant near-bottom flux towards the SSW (Guillén et al., 2002; Jiménez et al., 1999; Palanques et al., 2002). Taking into account these studies, the probability of occurrence of conditions exceeding the threshold for sediment entrainment was calculated by analysing long-term series of near-bottom wave-induced shear stress. Therefore, the probability of exceedance of such conditions was obtained by using a 18-year long wave time series

representative of the long-term wave climate (Fig. 2) recorded at a wave buoy deployed at 50 m depth in front of Cap Tortosa.

In addition to exceedance of threshold conditions, the other variable used to characterize sediment mobility was the “transport intensity parameter”, Φ . This parameter is estimated by assuming that near-bottom sediment transport is proportional to the excess bottom shear stress (or friction velocities) above the critical value. According to Madsen (1991), Sleath (1978) and Soulsby and Whitehouse (1997), we have assumed that bed load transport can be parameterized as a function of the shear stress to the 1.5 power (for non-cohesive sediments), i.e.

$$\Phi = \int (\tau - \tau_{cr})^{3/2} dt$$

where the integral indicates that the parameter is calculated for all wave conditions during a climatic year, which we obtained from the above-mentioned 18-year long record of wave data. Φ was calculated for both sediment sizes (0.125 mm and 0.063 mm). For the case of fine and cohesive sediments (< 0.063 mm), although there has been little agreement about the most appropriate formula to estimate bed erosion rates, most of existing formulas are also expressed in terms of an excess of shear stress above a threshold value (see review in Sanford and Maa, 2001). Among the different formulations, one of the most used is the linear one which permits limited and unlimited mud supply from the bottom, i.e.

$$E = M [\tau(t) - \tau_{cr}(m)]$$

where E is the mud erosion rate, M is the erosion rate parameter, $\tau(t)$ is the time-varying skin friction shear stress and $\tau_{cr}(m)$ is the critical shear stress which varies in vertical (m) in the bottom layer. This simple linear approach has been used by Sanford (2008) to build up a model to

simulate the erosion and deposition of fine sediments including consolidation, armoring and bioturbation processes. Strictly speaking, the transport intensity parameter should be applicable at depths shallower than the limit of the lobe front (18 m) where sandy sediment dominates, whereas E should be used at deeper waters where fine cohesive sediments dominate.

Finally, to assess where the sediment mobility can induce significant bottom changes, we also calculated the across-shelf distribution of sediment transport gradients ($\partial \Phi / \partial z$) since bottom change is proportional to local sediment transport gradients. This will only be valid for water depths where sandy sediments exist.

3.3 Wave propagation model

Wave propagation was simulated using the Mike-21 Parabolic Mild Slope (PMS) wave model (DHI, 1998). This numerical model solves the PMS equation and is capable of reproducing shoaling, refraction, dissipation due to bed friction and wave breaking, and diffraction. The bathymetry grid used in the wave propagation analysis was built re-sampling the high-resolution swath-bathymetry data at 20 m. Wave conditions utilised in the propagation analysis across the Sol de Riu lobe were representative of the most energetic conditions for the local wave climate and, especially, those able to impact on the coast in the Northern hemidelta. Thus, we simulated the propagation for the dominating ENE and E waves (Mendoza et al., 2011) with relatively long wave periods (5 s, 7 s, 9 s and 11 s). In a recent review of all existing wave data along the Catalan coast to characterize storms, Mendoza et al (2011) found that the most frequent wave storms are from the ENE and E sectors and they are characterized by the highest wave power content, with the largest ever recorded storms coming from both sectors.

4. Results

4.1 Seafloor and subsurface characters

The three beach system profiles in the study area have similar subaqueous slopes down to a water depth of about 7 m (Fig. 3). This common inner part is located within the depth range dominated by wave-breaking induced dynamics (Jiménez and Sánchez-Arcilla, 1993). At deeper locations, beach system profiles significantly differ depending on their location with respect to the lobe. The beach system profile named FAN, located at the turning point of El Fangar spit, off the relict lobe, is the steepest ($< 0.56^\circ$), with its distal segment even steeper (1.2°) than the inner one. Such a relatively steep profile is typical of accretionary sandy bodies, like spits, which are fed and built up by alongshore sediment transport. The southernmost beach system profile SRL cuts the central part of the lobe and displays two ridges at about 10-11 m water depth on top of a very gentle ($< 0.1^\circ$) distal segment that extends along 2.5 km. Below 12 m water depth, which is the wave base for short-period waves ($T_p = 4$ s), the slope becomes steeper (0.24°). The intermediate beach system profile INT is located over the northern part of the lobe and from 7 to 12 m water depth it is steeper than the SRL profile. INT profile becomes steeper at 13.5 m, where it reaches a slope of 0.24° . The latter value is found at only 12 m depth on the SRL profile.

Fig. 3

Swath bathymetry data demonstrates that the relict lobe consists of a large D-shaped sediment body with a well-defined and relatively smooth surface totalling 45 km^2 (Fig. 4A). The lobe is 7.8 km wide and has a gently sloping surface that extends 6.5 km north-eastwards (Fig. 4B). The flat lobe top extends down to a water depth of 18 m from where it drops off to deeper water with a slope angle ranging from 0.7° to 1.2° .

The top surface of the lobe shows more than 400 small-scale depressions down to 15 m water depth. The majority of these depressions are V-shaped with a maximum incision of 45 cm at their head (at the narrower section) (Fig. 4C). The depressions are 5-15 m wide, can reach up to 40 m in length and their long axis is generally oriented ENE-WSW to E-W. The deeper depressions are also observed on the acoustic backscatter intensity map and characterize by lower intensity of sound backscattered. It is rather common that two or more depressions coalesce and more than half are partially filled or smoothed. On the southern part of the relict lobe, numerous V-shaped bedforms delimit a large area with erosional steps of about 40 cm deep (Fig. 4A and D). A second type of depressions, linear in shape on the multibeam data occurs on the lobe front between 16 and 18 m water depth (Fig. 4A and E). They consist of two sets of E-W oriented straight and parallel furrows, 15-20 m wide and up to 375-500 m long. These furrows have a maximum depth of 25 cm and are spaced 85 to 140 m. On the backscatter map, each furrow is characterized by successive and equidistant (100 m) circular shapes (usually four) of lower backscattering intensity.

Fig. 4

The acoustic backscatter intensity map extracted from the 300 kHz swath-bathymetry data allowed us to identify four principal bottom types (Fig. 4E). Backscatter intensity for Sol de Riu relict lobe ranges between -44 and -24 dB. In general, the top surface of the relict lobe has an intermediate backscatter signature (-32 to -29 dB) down to 18-20 m in depth. The adjacent off-lobe area to the SE and, specially, the NW presents the lowest backscatter strength (-44 to -38 dB) while the highest intensity (-28 to -24 dB) is found on the gently sloping lobe downwards of 18-20 m water depth. The backscatter distribution can be roughly correlated to sediment grain size. This shows that the most prevailing sediment type yielding intermediate backscatter strength

for most of the relict lobe surface is sand dominated (e.g. samples 5 and 6 in Fig. 4E). On the shallowest part of the middle shoreface, between 10 and 12 m water depth, a compositional change is observed from sandy sediment (samples 2 to 4, 7 and 8) to more clayey and silty sediment (samples 11 to 14) yielding lower backscatter (-36 to -33 dB) than in the central section of the lobe. The adjacent off-lobe zone to the north is dominated by the finer fractions (sample 1) yielding the lowest backscatter in the study area. On the relict deltaic slope no sediment samples are available in this study for the highest backscatter intensity registered, however, previous studies determined that the sediment is essentially formed by mud and silt (Díaz et al., 1990, 1996). Backscatter data is thus quite variable and shows very high reflectivity values (-28 to -24 dB) for finer fractions at the slope of the lobe compared to backscattered intensities obtained in similar fractions (e.g. Hughes Clarke, 1993; Hughes-Clarke et al., 1996).

The boomer seismic reflection profiles show the internal structure of Sol de Riu relict lobe, which consists of a large number of seaward-oriented progradational sub-parallel reflectors. However, seismic penetration is practically lacking below the flat top central part and slope of the lobe, at least from 10 to 25 m water depth, where diffuse and chaotic seismic echoes and generally weak acoustic impedance contrasts mask the internal stratification of the lobe (generally below 1 m depth) (Fig. 5). In the deeper area, the presence of gas-charged sediments has been confirmed by Díaz et al. (1990).

Fig. 5

4.2. Sediment mobility

The annual percentage of exceedance of threshold conditions to mobilize sediments with diameters of 0.125 and 0.063 mm from 7.5 to 40 m depth is shown in Fig. 6A. These results evidence that the sediment at the lobe front will hardly be affected by the most frequent wave

conditions, which are dominated by short-period waves. This is reflected in the percentage of time that threshold conditions are exceeded at 18 m depth (15 % and 19 % for 0.125 and 0.063 mm, respectively). At 10 m depth the frequency of exceedance increases up to 34 % and 42 % for 0.125 and 0.063 mm, respectively. Although these values are quite high for the Mediterranean Sea, they are relatively low when compared to typical conditions on open ocean shelves where wave periods up to 25 s are not infrequent (Wright, 1995). The annual bedload sediment transport intensity curve for both sediment sizes follows the same pattern of very low values at the lobe front and a rapid increase at the shallower shoreface (Fig. 6A).

Fig. 6B shows the across-shelf distribution of sediment transport gradients ($\partial \Phi / \partial z$), which displays a sharp landwards-increasing pattern. According to the results obtained, the study area can be roughly divided into three depth zones in terms of sediment transport gradients. The deepest zone (Z3) corresponds to the relict deltaic slope, at depths in excess of 20 m, which experiences very small gradients in sediment transport intensity, indicating very small (if any) induced bottom changes. The intermediate zone (Z2), between 14 m and 20 m, corresponds to the outer relict deltaic plain, where transport gradient increases shoreward about 6 times faster than in the deepest part. This increase in gradient intensity should be reflected in higher sediment reworking, as well as in faster bottom changes in comparison with the relict deltaic slope Z3. Finally, the innermost area (Z1), at depths shallower than 14 m, corresponding to the inner relict deltaic plain, presents the largest transport intensity gradients and the fastest shoreward increase, which is about 5 times faster than the intermediate zone Z2 and 30 times faster than the deepest zone Z3. This pattern also indicates the expected magnitude of the potential bottom changes in this depth range in comparison with the deeper parts.

In addition to this, it has to be considered that the area of the lobe front is typical of shelves influenced by the presence of a river mouth, with a convex profile with bottom slope increasing seawards. This will induce a downward increase in the component of the gravity force and, in

consequence, a potential increase in the sediment-gravity flow if present (e.g. Wright and Friedrichs, 2006). The highest bottom slopes are found in the front part of the lobe between 18 m and 30 m deep, where as it was mentioned before, the sediment is essentially formed by mud and silt. The combination of relative deep waters (in comparison with typical wave lengths) and cohesiveness, makes this sediment to be rather stable, although they could be mobilized under storm events, when near-bottom shear stress drastically increases. Under these favourable conditions, fine sediment resuspension could create thin near-bed layers susceptible to move downslope (e.g. Traykovski et al. 2007; Wright et al., 2001). In this sense, it has to be noted that local maximum values of the bottom slope ($\sin \theta$) along the lobe front are between 0.01 and 0.015 (between 18 m and 30 m deep), which are in the order of magnitude of typical critical slopes (0.01-0.02) where gravity flows may be self-sustained by auto suspension (Friedrichs and Wright, 2004). At deeper waters, the bottom slope rapidly decreases below 0.01 and, this together the decrease in wave and current induced-stresses should contribute to sediment deposition of these sediments.

Fig. 6

4.3 Wave propagation

The effects of wave propagation over Sol de Riu relict lobe have been modeled for conditions equivalent to the most severe coastal storms, when T_p increases from 5 s up to 11 s with two main directions, from ENE and E. As an example, Fig. 7 shows the wave height amplification factor under storm conditions ($T_p = 11$ s, ENE), which is given by the ratio of local wave height at any location with respect to its value in deep waters. The larger the value is, the higher the local wave will be. As it can be seen, along most of the northern hemidelta coast, the wave height does not vary significantly with the exception of the stretch northwards of the subaqueous Sol de Riu

lobe where a drastic wave height increase is observed. Fig. 8 summarizes the alongshore wave height distribution for incident wave periods ranging from 5 s to 11 s. It shows that waves with periods shorter than 5 s are not significantly affected by the presence of the relict lobe or, at least, no significant alongshore gradient in wave conditions is observed. However, for relatively long-period waves ($T_p \geq 7$ s) the influence of the lobe on their propagation is clearly noticed, resulting in a concentration of wave energy (increasing H_s) in its northern part and the adjacent shoreline. The increase in wave energy gets larger along with the wave period. In the Catalan coasts in general and, in the Ebro Delta in particular, relatively long-period waves ($T_p > 9$ s) are mainly generated under storm conditions (Jiménez et al., 1997). Although the frequency of occurrence of these long-period waves is small (about 11%), they contribute with about 27% of the total power content of local wave climate (Fig. 9). Wave propagation results show that the relict lobe has a stronger influence on wave height distribution along the shoreline for E and ENE long-period waves ($T_p \geq 9$ s) where the H_s increase is mainly concentrated in the northern part of the investigated shoreline, with the lowest energy content in its northernmost end due to the sheltering effect of the subaqueous lobe (Fig. 7).

Fig.7

Fig.8

Fig.9

5. Discussion

According to Maldonado (1986) and Somoza et al. (1998) the Sol de Riu lobe was active between 1350 and 1700 AD. Our results show that under present conditions the **shallow shoreface** (i.e., at depths shallower than about 7 m) is probably the most dynamic part of the relict lobe in terms of wave-induced bottom shear stress and, consequently also in terms of

sediment mobility. Therefore, the shallowest part of the relict lobe is the most prone to significant morphological change, both in magnitude and in rate. Seabed modifications are large (i.e., largest intensity of sediment reworking) and occur at seasonal time scales. They are mainly controlled by wave-induced alongshore and cross-shore dynamics, especially during major storm events. In this shallowest part of the shoreface, the bottom slope is almost alongshore uniform (Fig. 3) due to the continuous action of wave-induced littoral dynamics. This zone is limited at its deepest end by the depth of closure, which in this area is around 7 m (Jiménez and Sánchez-Arcilla, 1993). This concept, usually employed in coastal engineering, refers to the depth where beach profile changes become insignificant at yearly scale (Hallermeier, 1981). However, as it can be clearly seen from sediment mobility values, this does not imply that bottom sediment is at rest and, in fact, the probability of mobility is larger than 40 % (Fig. 6). Although at these depths, induced transport rates generate significant bottom changes at yearly scales, when integrated over longer time periods (decades) their cumulative impact should be visible. In this sense, Jiménez et al. (2011) found shoreface bottom changes down to 10 m deep when comparing beach profiles separated by a period of 20 years.

In the **middle shoreface** extending down to about 15 m water depth, cumulative sediment transport has reworked the original relict lobe deposits thus inducing significant morphology and depth changes since the Sol de Riu lobe was abandoned and stopped accreting. Therefore, the modern shape and bathymetry of the lobe are the consequence of sediment transport during at least the last three centuries. Assuming that the wave-induced skin friction is the main driver of near-bottom sediment dynamics, in an average climatic year the middle shoreface is active between 25 % and 40 % of the time. According to the estimated transport regime, the wave-induced skin friction could be active enough to erase or partially erode during a climatic year the shallow V-shaped depressions and the erosional steps identified in the swath-bathymetry data (Fig. 4). Because gas-charged (gassy) sediments and pockmarks have been identified along the

Ebro River and offshore the Ebro Delta (Díaz et al., 1990; Maestro et al., 2002), the potential relation of the shallow V-shaped depressions and the erosional steps with the presence of subsurface gas is examined. The seismic reflection profiles show the presence of very narrow acoustic maskings and acoustic turbidity zones (amorphous echoes) represented by significant disruptions caused by scattering and higher attenuation of the seismic energy probably due to free gas present within the sediments of the relict Sol de Riu lobe. The gas is believed to be largely of biogenic origin, resulting from the decay of organic matter trapped in old deltaic sediments that accumulated at much higher rates than at present (Díaz et al., 1990). The front of the gas-charged sediments is found very close to the seafloor, generally below 1 m from the seabed (Fig. 5), however no distinct morphological expressions (e.g. cone-shaped acoustic masking features) or seepages, usually easily detected by geo-acoustic systems, have been found to confirm near-surface gas release at the location of the Sol de Riu lobe and nearby areas. In addition, none of the features observed on the seafloor of the relict lobe have the rounded or oval shape of typical gas seeping structures such as pockmarks. On the other hand, the anthropogenic hypothesis for this disturbed seabed is supported by the orientation pattern of the shallow depressions, which is thought to be related to the movement of boat anchoring chains and ropes going back and forth following the direction of the dominant ENE to E winds. The V shape of the depressions points to the triangular metal anchors typically utilised in the area. We argue that dense concentrations of these man-made depressions, such as those on the southern part of the lobe, could lead to the removal of unconsolidated sediment and the formation of erosional steps. This implies that the persistence of anchor marks is essentially seasonal and the fresh-looking ones (less than half of them) observed on the seabed map would have been generated during the same year as in which the swath-bathymetry data were acquired, likely by mid-size leisure and tourist boats targeting La Marquesa beach and nearby places in summer months. Therefore, although we consider the possibility of existence of seepages, we rule out the

probability that the shallow V-shaped depressions and the erosional steps are caused by gas seepage through the seabed. Instead, these bedforms are seen as the footprint of human activities, as boat anchoring. It has to be noted that although sediment resuspension in this area is essentially wave-induced driven, the intensity of sediment mixing in the water column is mainly dominated by the vertical structure of the currents (Guillén et al. 2002; Jiménez et al. 2002). With respect to this, whereas skin friction (grain-roughness) is the relevant parameter for sediment remobilisation, the vertical structure of currents will be controlled by bottom roughness and, in consequence, by any component contributing to it (e.g. Nielsen, 1992). Thus, bedforms such as ripples will control the magnitude of form drag roughness which is significantly larger than the grain-related one. Although no experimental data on bottom roughness in the area do exist, Guillén et al. (2002) estimated ripple development on the middle shoreface (at 8.5 m and 12.5 m deep) in the Ebro delta during the onset of a eastern wave storm using the Wiberg and Harris (1994) model. They calculated that maximum ripple heights during such conditions up to 1.6 cm and 1.3 cm respectively for both locations, which were consistent with the required ones to reproduce measured current profiles. In addition to this, other factors such as biological ones may also contribute to bottom roughness. In the southern part of the Ebro delta, Guillén et al. (2008) reported the local effect of biological activity on bottom roughness. These authors detected ripples disappearance due to the action of *Ophiura ophiura* during fairweather conditions (very weak bottom stress) which induced a high rate of bioturbation. Under these conditions, the bottom roughness passed from being controlled by ripples to be controlled by biological roughness.

The **deep shoreface** develops at depths larger than 15 m and corresponds to the relict lobe front. It is characterized by very low sediment mobility in terms of both frequency of exceedance of threshold conditions (about a 5 % at 30 m depth) and sediment transport rates. Sediment transport gradients are very small and, consequently, bottom change with respect to former

ambient conditions should be also very small. The furrows observed on the front of the lobe are most probably trawling marks (Fig. 4A). Such marks are common on the Catalan continental shelf and have been also observed at depths less than 50 m depth off Besòs and Llobregat river mouths nearby Barcelona (Liquete et al., 2007). Because of the very small estimated potential sediment mobility at depths larger than 15 m, bottom trawling marks mapped between 16 and 18 m water depth could be from several years to a few decades old. Bottom trawling at depths less than 50 m was banned in Spain in year 1975.

5.1 High backscatter on the slope of the lobe

Backscatter differences in the study area are likely caused by variations in sediment properties such as grain-size distribution, roughness and bioturbation, or to compaction effects (Blondel and Murton, 1997; Collier and Brown, 2005; Goff et al., 2000; Urgeles et al., 2002). However, the general high acoustic multibeam backscatter values on the slope of the lobe (deeper than 18-20 m water depth) are not the result of the grain-size of the sediment and it is unlikely that the acoustic turbidity associated to the presence of shallow gas generally observed below 1 m depth (gas front on the high-resolution reflection seismic profiles, Fig. 5) can affect the backscatter strength of this area. Previous studies suggested that the presence of free gas in the subsurface sediments (first ~ 20 cm) influences the acoustic properties of the sediment amplifying the energy scattering because of the increased acoustic impedance (e.g. Boyle and Chotiros, 1995; Fonseca et al., 2002; Hagan and Vogt, 1999; Naudts et al., 2008; Sweeney et al., 2012), although, Fonseca et al. (2002) postulated that in shallow water the presence of free gas in the subsurface sediments reduces the backscatter intensity due to the decrease in sediment sound speed. High-resolution reflection seismic systems are significantly affected by the presence of shallow gas and are commonly used for the detection of free gas in sediments (e.g. Anderson and Hampton, 1980). There are two major reasons that could explain why free gas in the upper

centimetres of the surface sediment of the slope is not detected on the boomer seismic profiles: 1) the quality of the data suffered from a combination of several acquisition parameters (Naudts et al., 2009) and 2) the source frequency of the boomer is not the right one to identify small amounts of gas in subsurface sediments, depending also on the concentration, physical parameters and distribution of the gas. Mathys et al. (2005) investigated the expression of gas bubbles on reflection seismic profiles of two distinct frequency ranges using a boomer (600-2600 Hz) and an echosounder (38 kHz) to conclude that both seismic sources showed strong differences in displaying reflectors where the boomer profile shows a downward shift (deeper location) indicating a velocity dispersion (a difference in arrival time). The authors shown as well that free gas could be also present in non-turbidity zones on seismic profile when the amount is too small to produce seismic scattering. Naudts et al. (2009) used also different high-resolution reflection seismic systems with different signal spectra and concluded that the higher frequencies provide a higher-resolution image of the subsurface and consequently the most valuable information about the depth of the shallow gas present in the sediments. This suggest that a low amount of free gas can go undetected on the high-resolution seismic data, as the source frequency of the boomer (dominant frequency 3-4 kHz) may be not high enough to identify small amounts of gas in subsurface sediments, depending also on the concentration, physical parameters and distribution of the gas bubbles. We can thus expect that small amounts of free gas, derived from gas-charged subsurface sediments, cause an increase in the backscatter amplitude, although in amounts and migration rates that are too low to lead to the formation of pockmarks on the seabed.

According to Sills and Wheeler (1992), gas-charged sediments in the subsurface usually lead to lowered shear strength at the seabed than equivalent deposits without gas, which has the potential to result in the extension of sediment instability and coastal erosion. Possibly, sediment mobility at the slope of the Sol de Riu lobe is influenced by the presence of free gas in the sub-

surface sediment to an extent that we are unable to quantify. Amongst other effects it should be expected that free gas influences the cohesion of the sediment easing the removal action of the wave-induced dynamics.

5.2. Role of the relict lobe on deltaic evolution and present-day coastal processes

Following the abandonment of the Sol de Riu lobe around 1700 AD in response to the opening of a new mouth of the Ebro River southwards of the present one (Somoza et al. 1998), it was subsequently reshaped by sediment erosion and redistribution along the coast. The erosion of the abandoned lobe provided sediment for the development of subaqueous sand bars, beaches and El Fangar spit (Maldonado, 1977). During the initial stage, the partial dismantling of the lobe likely was related mainly to wave-induced littoral dynamics. Assuming that no significant variation in wave climate has occurred since the lobe was abandoned, ENE and E waves (Fig. 2) should have acted as the dominant forcing mechanism generating a net northward alongshore sediment transport leading to the build-up of El Fangar spit. Likely, in the first stages this process was very fast, eased by the orientation of the shoreline with respect to the dominant incident waves from the east. It is also likely that lobe dismantling slowed down in parallel with the re-orientation of the coastline while the protruding tip of the lobe itself and the upper younger and unconsolidated sedimentary units continued being eroded. A rather recent event illustrates how fast coastal retreat and re-orientation, and spit formation, could be. When the youngest active deltaic lobe, the Buda lobe (Fig. 1), was abandoned in the mid 20th century, the shoreline retreated up to 2 km in only 50 years. Retreat rates of Buda lobe decreased from about $70 \text{ m}\cdot\text{y}^{-1}$ during the 1957-73 period to $10 \text{ m}\cdot\text{y}^{-1}$ during the last decades (Jiménez and Sánchez-Arcilla, 1993; Valdemoro et al., 2007).

The bathymetry of the Sol de Riu lobe shows that contour lines run parallel to the shoreline only down to 12 m water depth, where the middle shoreface is. This means that incident waves

with periods ≤ 5 s, which correspond to a wavelength of about 30 m, move unaffected by the lobe bulge, subsequently inducing alongshore uniform wave conditions in the study area. These waves represent about 26 % of the effective waves (i.e. those able to impact this coastal stretch, see Fig. 9) and its power content ($\sim Hs^2$) is only 7 % of the total power content of incident waves. Thus, waves unaffected by the presence of the relict lobe are restricted to low energy ones, which are of lower significance for the long-term evolution of the shoreline. At 18-20 m water depth, near the edge of the lobe front (Fig. 4), the lobe outbuilding significantly affects waves with peak periods equal or larger than 7 s. These wave conditions represent about 29 % of the effective waves and they encompass about 55 % of the power content (Fig. 9). In other words, the presence of the relict lobe bulge directly affects the most energetic wave conditions in the study area, which usually occur between October and March every year (Jiménez et al. 1997). Under these conditions, sediment transport rates increase northwards thus inducing an alongshore gradient that largely explains the long-term shoreline erosion of La Marquesa beach. Moreover, the significant local increase in wave height in the northern part of the deltaic coast (Figs. 7 and 8) coincides with the area that usually is more severely affected by eastern storms.

Therefore, the presence of Sol de Riu relict lobe attached to the northern hemidelta significantly influences wave-induced littoral dynamics since it modifies the wave propagation pattern with respect to a hypothetical situation without the lobe. As a consequence, the subaqueous relict lobe determines the evolution of the entire shoreline in the study area. Fig. 10 shows long-term averaged shoreline displacement rates along the northern hemidelta coast, excluding El Fangar spit, during the 1957-2007 period. The erosional character of the coastline appears clearly, with a spatially averaged long-term erosion rate of about $5 \text{ m}\cdot\text{y}^{-1}$. This erosional behaviour has been associated to alongshore sediment transport induced by the dominant eastern wave climate (Jiménez and Sánchez-Arcilla, 1993). The net alongshore sediment transport pattern is directed northwards in the study area and such gradient should imply

northwards increasing transport rates (Jiménez and Sánchez-Arcilla, 1993). Such an alongshore sediment transport pattern is only possible from alongshore non-uniform wave conditions, which are mainly controlled by the presence of the subaqueous Sol de Riu relict lobe.

Fig. 10

6. Conclusions

We analysed the detailed morphology of the relict subaqueous Sol de Riu lobe located in front of La Marquesa beach, and assess its role in controlling present-day coastal dynamics. Our results characterize the Sol de Riu lobe as a prominent D-shaped bulge in erosion that played and continues to play, after it was abandoned, a very significant role in the morphological evolution of the northern hemidelta coast.

The morphology of the lobe between ~ 9 to 15 m water depth is characterized by a large number of oriented V-shaped depressions attributed to boat anchoring. Jointly with local bottom trawling marks at the front of the lobe, these bedforms illustrate the most common direct anthropogenic impact on the seafloor of the lobe. Estimations of the mobility of bottom sediment showed that the shallow shoreface is the most dynamic part of the lobe in terms of wave-induced bottom shear stress and therefore in morphological change at a seasonal time scale. The middle shoreface is active between 25 % and 40% of a climatic year and probably effective enough to erase or partially erode seasonally the footprint of boat anchoring. The deep shoreface, at depths larger than 15 m, is characterized by very small estimated potential sediment mobility that imply very limited bottom change.

Other relevant elements are the current situation of the Sol de Riu relict lobe in terms of sedimentary equilibrium (erosion vs. steady state) and its influence on coastal sediment dynamics and the evolution of the deltaic shoreline. The temporal analysis of the sediment transport regime

shows that down to 15 m water depth the relict lobe is eroding, particularly during the most energetic wave conditions generally occurring between October and March every year when eastern storms lash out. Wave propagation scenarios illustrate that with augmenting wave periods, the lobe bulge increasingly affects wave refraction and leads to larger wave heights in the northern part of the investigated coastline which contributes to the long-term shoreline erosion observed along La Marquesa beach in the northern hemidelta coast. In other words, the subaqueous relict lobe determines the evolution of the entire shoreline in the study area.

A better understanding, management and preservation of this valuable coastal stretch would require undertaking a systematic monitoring of its morphological evolution and grain size variation, and a dedicated study of the role of free gas in the subsurface sediments on sediment erosion and mobility.

Acknowledgements

Fieldwork was supported by the EU EURODELTA (EVK3-2001-00033), and the Spanish PRODELTA (REN2002-02323) and GRACCIE (CSD2007-00067) research projects. *Direcció General de Pesca i Afers Marítims* of Generalitat de Catalunya provided the *Arraix* survey boat. Special thanks are given to the master of *Arraix* and the shipboard party for their help during data collection. C. Lavoie was funded by a postdoctoral fellowship from *Fonds Québécois de recherches sur la Nature et les Technologies* (FQRNT) of the Québec government (Canada), and side funds by Universitat de Barcelona. The work of J.A. Jiménez was done in the framework of the VuCoMA (CTM2008 05597/MAR) and PaiRisC-M (CTM2011-29808 research projects funded by the Spanish Ministry of Science and Innovation (CTM2008-05597/MAR and CTM2011-29808). GRC Geosciences is supported by Generalitat de Catalunya Excellence grant 2009-SGR-1305.

References

- Alvarado-Aguilar, D., Jiménez, J.A., Nicholls, R.J., 2012. Flood hazard and damage assessment in the Ebro Delta (NW Mediterranean) to relative sea level rise. *Natural Hazards* 62, 1301-1321.
- Anderson, A.L., Hampton, L.D., 1980. Acoustics of gas-bearing sediments I. Background. *Journal of the Acoustical Society of America* 67, 1865-1889.
- Blondel, P., Murton, B.J., 1997. *Handbook of Seafloor Sonar Imagery*. Wiley-Praxis Series in Remote Sensing. John Wiley and Sons Ltd. in association with Praxis Publishing Ltd., Chichester. 314 pp.
- Bolaños, R., Sánchez-Arcilla, A., 2006. A note on nearshore wave features: Implications for wave generation. *Progress in Oceanography* 70, 168-180.
- Boyle, F.A., Chotiros, N.P., 1995. A model for acoustic backscatter from muddy sediments. *Journal of the Acoustical Society of America* 98, 525-530.
- Canals, M., Casamor, J.L., Urgeles, R., Farrán, M., Calafat, A.M., Amblas, D., Willmott, V., Estrada, F., Sánchez, A., Arnau, P., Frigola, J., Colàs, S., 2004. *Mapa del relleu submarí de Catalunya*. Institut Cartogràfic de Catalunya, Barcelona. 1:250 000.
- Collier, J.S., Brown, C.J., 2005. Correlation of sidescan backscatter with grain size distribution of surficial seabed sediments. *Marine Geology* 214, 431-449.
- DHI, 1998. Mike 21 parabolic mid-slope waves module. User guide and Reference Manual.
- Díaz, J.I., Nelson, C.H., Barber Jr., J.H., Giró, S., 1990. Late Pleistocene and Holocene sedimentary facies on the Ebro continental shelf. *Marine Geology* 95, 333-352.
- Díaz, J.I., Palanques, A., Nelson, C.H., Guillén, J., 1996. Morpho-structure and sedimentology of the Holocene Ebro prodelta mud belt (northwestern Mediterranean Sea). *Continental Shelf Research* 16, 435-456.

- Dunbar, G.B., Barrett, P.J., 2005. Estimating palaeobathymetry of wave-graded continental shelves from sediment texture. *Sedimentology* 52, 253-269.
- Durand, N., Fiandrino, A., Fraunié, P., Ouillon, S., Forget, P., Naudin, J.J., 2002. Suspended matter dispersion in the Ebro ROFI: an integrated approach. *Continental Shelf Research* 22, 267-284.
- Fonseca, L., Mayer, L., Orange, D., Driscoll, N., 2002. The high-frequency backscattering angular response of gassy sediments: Model/data comparison from the Eel River Margin, California. *Journal of the Acoustical Society of America* 111, 2621-2631.
- Friedrichs, C.T., Wright, L.D., 2004. Gravity-driven sediment transport on the continental shelf: implications for equilibrium profiles near river mouths. *Coastal Engineering* 51, 795-811.
- García, M.A., Sánchez-Arcilla, A., Sierra, J.P., Sospedra, J., Gómez, J., 1993. Wind waves off the Ebro Delta, NW Mediterranean. *Journal of Marine Systems* 4, 235-262.
- George, D.A., Hill, P.S., 2008. Wave climate, sediment supply and the depth of the sand-mud transition: A global survey. *Marine Geology* 254, 121-128.
- Goff, J.A., Olson, H.C., Duncan, C.S., 2000. Correlation of side-scan backscatter intensity with grain-size distribution of shelf sediments, New Jersey margin. *Geo-Marine Letters* 20, 43-49.
- Guillén, J., Jiménez, J.A., 2009. Reply to the Comment on 'Wave climate, sediment supply and the depth of the sand-mud transition: A global survey' by D.A. George and P.S. Hill. *Marine Geology* 264, 258-261.
- Guillén, J., Palanques, A., 1997. A historical perspective of the morphological evolution in the lower Ebro river. *Environmental Geology* 30, 174-180.
- Guillén, J., Jiménez, J.A., Palanques, A., Gracia, V., Puig, P., Sánchez-Arcilla, A., 2002. Sediment resuspension across a microtidal, low-energy inner shelf. *Continental Shelf Research* 22, 305-325.

- Guillén, J., Soriano, S., Demestre, M., Falqués, A., Palanques, A., Puig, P., 2008. Alteration of bottom roughness by benthic organisms in a sandy coastal environment. *Continental Shelf Research* 28, 2382-2392.
- Hagen R.A., Vogt, P.R., 1999. Seasonal variability of shallow biogenic gas in Chesapeake Bay. *Marine Geology* 158, 75-88.
- Hallermeier, R.J. 1981. A profile zonation for seasonal sand beaches from wave climate. *Coastal Engineering* 4, 253-277.
- Hughes Clarke, J.E., 1993. The potential for seabed classification using backscatter from shallow water multibeam sonars. In: Pace, N., Langhorne, D.N. (Eds.), *Acoustic Classification and Mapping of the Seafloor*. *Proceedings of the Institute of Acoustics* 15, 381–388.
- Hughes-Clarke, J.E., Mayer, L.A., Wells, D.E., 1996. Shallow-water imaging multibeam sonars: A new tool for investigating seafloor processes in the coastal zone and on the Continental Shelf. *Marine Geophysical Researches* 18, 607-629.
- Jiménez, J.A., Guillén, J., Gracia, V., Palanques, A., García, M.A., Sánchez-Arcilla, A., Puig, P., Puigdefàbregas, J., Rodríguez, G., 1999. Water and sediment fluxes on the Ebro Delta shoreface: on the role of low frequency currents. *Marine Geology* 157, 219-239.
- Jiménez, J.A., Guillén, J., Sánchez-Arcilla, A., Gracia, V., Palanques, A., 2002. Influence of benthic boundary layer dynamics on wind-induced currents in the Ebro delta inner shelf. *Journal of Geophysical Research: Oceans* 107, 3054.
- Jiménez, J.A., Sánchez-Arcilla, A., 1993. Medium-term coastal response at the Ebro delta, Spain. *Marine Geology* 114, 105-118.
- Jiménez, J.A., Sánchez-Arcilla, A., Bou, J., Ortiz, M.A., 1997a. Analysing short-term shoreline changes along the Ebro Delta (Spain) using aerial photographs. *Journal of Coastal Research* 13, 1256-1266.

- Jiménez, J.A., Sánchez-Arcilla, A., Valdemoro, H.I., Gracia, V., Nieto, F., 1997b. Processes reshaping the Ebro delta. *Marine Geology* 144, 59-79.
- Jiménez, J.A., Sancho-García, A., Bosom, E., Valdemoro, H.I., Guillén, J., 2012. Storm-induced damages along the Catalan coast (NW Mediterranean) during the period 1958–2008. *Geomorphology* 143-144, 24-33.
- Jiménez, J.A., Valdemoro, H.I., Alvarado, D., Gracia, V., 2011. Estudio y análisis de alternativas de actuación y gestión del frente costero del Delta del Ebro. Laboratori d'Enginyeria Marítima, Barcelona.
- Liquete, C., Canals, M., Arnau, P., Urgeles, R., Durrieu de Madron, X., 2004. The impact of humans on strata formation along Mediterranean margins. *Oceanography* 17, 42-51.
- Liquete, C., Canals, M., Lastras, G., Amblas, D., Urgeles, R., De Mol, B., De Batist, M., J.E., H.-C., 2007. Long-term development and current status of the Barcelona continental shelf: A source-to-sink approach. *Continental Shelf Research* 27, 1779-1880.
- Liquete, C., Lucchi, R.G., Garcia-Orellana, J., Canals, M., Masque, P., Pasqual, C., Lavoie, C., 2010. Modern sedimentation patterns and human impacts on the Barcelona continental shelf (NE Spain). *Geologica Acta* 8, 1-19.
- Maa, J.P.-Y., Sanford, L., Halka, J.P., 1998. Sediment resuspension characteristics in Batimore Harbor, Maryland. *Marine Geology* 146, 137-145.
- Madsen, O.S., 1991. Mechanics of cohesionless sediment transport in coastal waters. *Proceedings of Coastal Sediments '91*, 15-26.
- Madsen, O.S., Grant, W., 1976. Quantitative description of sediment transport by waves. *Proceedings of Coastal Engineering '76*, 1093-1112.
- Maestro, A., Barnolas, A., Somoza, L., Lowrie, A., Lawton, T., 2002. Geometry and structure associated to gas-charged sediments and recent growth faults in the Ebro Delta (Spain). *Marine Geology* 186, 351-368.

- Maldonado, A., 1972. El delta del Ebro, estudio sedimentológico y estratigráfico. Ph.D. Thesis, Universitat de Barcelona, 475 pp.
- Maldonado, A., 1975. Sedimentation, stratigraphy and development of the Ebro Delta, Spain. In: Brossard, M.L. (Ed.), Delta models for exploration. Houston Geological Society, Texas, pp. 311-338.
- Maldonado, A., 1977. Introducción geológica al delta del Ebro: Geological introduction to the Ebro Delta. Treballs de la Institució Catalana d'Història Natural 8, 7-45.
- Maldonado, A., 1986. Sedimentary environments and evolution of the Ebro Delta. *Thalassas* 4, 151-161.
- Maldonado, A., Riba, O., 1971. El delta reciente del río Ebro: descripción de ambientes y evolución. *Acta Geológica Hispánica* VI, 131-138.
- Mathys, M., Thießen, O., Theilen, F., Schmidt, M., 2005. Seismic characterisation of gas-rich near surface sediments in the Arkona Basin, Baltic Sea. *Marine Geophysical Researches* 26, 207-224.
- Mendoza, E.T., Jiménez, J.A., Mateo, J., 2011. A coastal storms intensity scale for the Catalan sea (NW Mediterranean). *Natural Hazards and Earth System Sciences* 11, 2453-2462.
- Naudts, L., De Batist, M., Greinert, J., Artemov, Y., 2009. Geo- and hydro-acoustic manifestations of shallow gas and gas seeps in the Dnepr paleodelta, northwestern Black Sea. *The Leading Edge* 28, 1030-1040.
- Naudts, L., Greinert, J., Artemov, Y., Beaubien, S.E., Borowski, C., De Batist, M., 2008. Anomalous sea-floor backscatter patterns in methane venting areas, Dnepr paleo-delta, NW Black Sea. *Marine Geology* 251, 253-267.
- Nielsen, P., 1992. Coastal bottom boundary layer and sediment transport. World Scientific, Singapore, 324 pp.

- Palanques, A., Plana, F., Maldonado, A., 1990. Recent influence of man on the Ebro margin sedimentation system, northwestern Mediterranean. *Marine Geology* 95, 247-263.
- Palanques, A., Puig, P., Guillén, J., Jiménez, J.A., Sánchez-Arcilla, A., Madsen, O. 2002. Near-bottom suspended sediment fluxes on the microtidal low-energy Ebro continental shelf (NW Mediterranean). *Continental Shelf Research* 22, 285-303.
- Sánchez-Arcilla, A., Jiménez, J.A., García, M.A., Stive, M.J.F., 1993. Vulnerability of low-lying coasts to climatic events: the Ebro delta case, US-Spain Workshop on Natural Hazards, Barcelona, pp. 257-331.
- Sánchez-Arcilla, A., Jiménez, J.A., Stive, M.J.F., Ibañez, C., Pratt, N., Day Jr., J.W., Capobianco, M., 1996. Impacts of sea-level rise on the Ebro delta: a first approach. *Ocean and Coastal Management* 30, 197-216.
- Sanford, L.P. 2008. Modeling a dynamically varying mixed sediment bed with erosion, deposition, bioturbation, consolidation, and armoring. *Computers & Geosciences* 34, 1263-1283.
- Sanford, L.P., Maa, J.P.-Y., 2001. A unified erosion formulation for fine sediments. *Marine Geology* 179, 9-23.
- Sills, G.C., Wheeler, S. J., 1992. The significance of gas for offshore operations. *Continental Shelf Research* 10, 1239-1250.
- Sleath, J.F.A., 1978. Measurements of bed load in oscillatory flow. *Journal of the Waterway Port Coastal and Ocean Division* 104, 291-307.
- Somoza, L., Barnolas, A., Arasa, A., Maestro, A., Rees, J.G., Hernández-Molina, F.J., 1998. Architectural stacking patterns of the Ebro delta controlled by Holocene high-frequency eustatic fluctuations, delta-lobe switching and subsidence processes. *Sedimentary Geology* 117, 11-32.

- Soulsby, R.L., Whitehouse, R.J.S.W., 1997. Threshold of sediment motion in coastal environments, Proceedings of the Pacific Coasts and Ports '97 Conference, University of Canterbury, Christchurch, pp. 149-154.
- Sweeney, E.M., Gardner, J.V., Johnson, J.E., Mayer, L.A., 2012. Geological interpretation of a low-backscatter anomaly found on the New Jersey continental margin. *Marine Geology* 326-328, 46-54.
- Traykovski, P., Wiberg, P.L., Geyer, W.R., 2007. Observations and modeling of wave-supported sediment gravity flows on the Po prodelta and parison to prior observations from the Eel shelf. *Continental Shelf Research* 27, 375-399.
- Urgeles, R., Locat, J., Schmitt, T., Hughes-Clarke, J.E., 2002. The July 1996 flood deposit in the Saguenay Fjord, Quebec Canada: implications for sources of spatial and temporal backscatter variations. *Marine Geology* 184, 41-60.
- Valdemoro, H.I., Sánchez-Arcilla, A., Jiménez, J.A., 2007. Coastal dynamics and wetlands stability. The Ebro delta case. *Hydrobiologia* 577, 17-29.
- Varela, J.M., Gallardo, A., Lopez de Velasco, A., 1986. Retención de sólidos por las presas de Mequinenza y Ribarroja. Efectos en los aportes al delta del Ebro, in: Mariño, M. (Ed.), El sistema integral del Ebro: cuenca, delta y ambiente marino. Hermes, Madrid, Spain, pp. 203-219.
- Wiberg, P., Harris, C.K., 1994. Ripples geometry in wave-dominated environments. *Journal of Geophysical Research* 99, 775-789.
- Wolanski, E., Fabricius, K., Spagnol, S., Brinkman, R., 2005. Fine sediment budget on an inner-shelf coral-fringed island, Great Barrier Reef of Australia. *Estuarine, Coastal and Shelf Science* 65, 153-158.
- Wright, L.D., 1995. Morphodynamics of inner continental shelves. CRC Press, Boca Raton.

Wright, L.D., Friedrichs, C.T., 2006. Gravity-driven sediment transport on continental shelves: A status report. *Continental Shelf Research* 26, 2092-2107.

Wright, L. D., Friedrichs, C. T., Kim, S. C., Scully, M.E. 2001. Effects of ambient currents and waves on gravity-driven sediment transport on continental shelves. *Marine Geology* 175, 25-45.

Figures

Fig. 1. A. General map of the Ebro Delta and nearby terrestrial and marine areas showing the swath-mapped area and the location of beach system profiles, single channel 200J boomer seismic reflection profiles and sediment samples used for this study. The location of modern (Buda) and relict (Riuet Vell, Migjorn and Sol de Riu) lobes off the present deltaic shoreline is also shown. Isobath interval is 5 m (Canals et al., 2004). Location of Figs. 4 and 5 is provided. Land orthophoto courtesy of *Institut Cartogràfic de Catalunya*. **B.** Close-up of La Marquesa beach in the Northern hemidelta coast (Landsat image 1996). **C.** Aerial side-looking photograph illustrating noticeable shoreline erosion along La Marquesa beach after the impact of a storm with long-period eastern waves ($T_p \geq 13s$) in November 2001.

Fig. 2. A. Directional distribution of wave peak periods in the study area. **B.** Significant wave height off the Ebro Delta during the 1990-2008 period.

Fig. 3. Beach system profiles in the area of the relict Sol de Riu lobe with slope values in degrees. MSL: mean sea level. Land orthophoto courtesy of *Institut Cartogràfic de Catalunya*.

Fig. 4. A. Shaded relief image of Sol de Riu relict lobe. **B.** Slope gradient map of Sol de Riu relict lobe. **C.** Close-up on V-shaped depressions. **D.** Close-up on irregular erosional steps (blue arrows) also showing V-shaped depressions nearby. Contour equidistance in A and B is 2 m. **E.** Backscatter strength map of the Sol de Riu relict lobe and grain size distribution from seafloor sediment samples. High backscatter intensity is represented by light colours and low backscatter intensity by dark colours. See location in Fig. 1.

Fig. 5. Boomer 200 J single channel seismic reflection profile showing diffuse and chaotic seismic echoes masking the internal stratification at the front Sol de Riu lobe. See location in Fig. 1. TWT (ms): Two-way travel time (in milliseconds).

Fig. 6. A. Across-shelf distribution of the annual percentage of exceedance of threshold conditions and annual bed-load transport intensity for 0.125 and 0.063 mm sediment grain size.

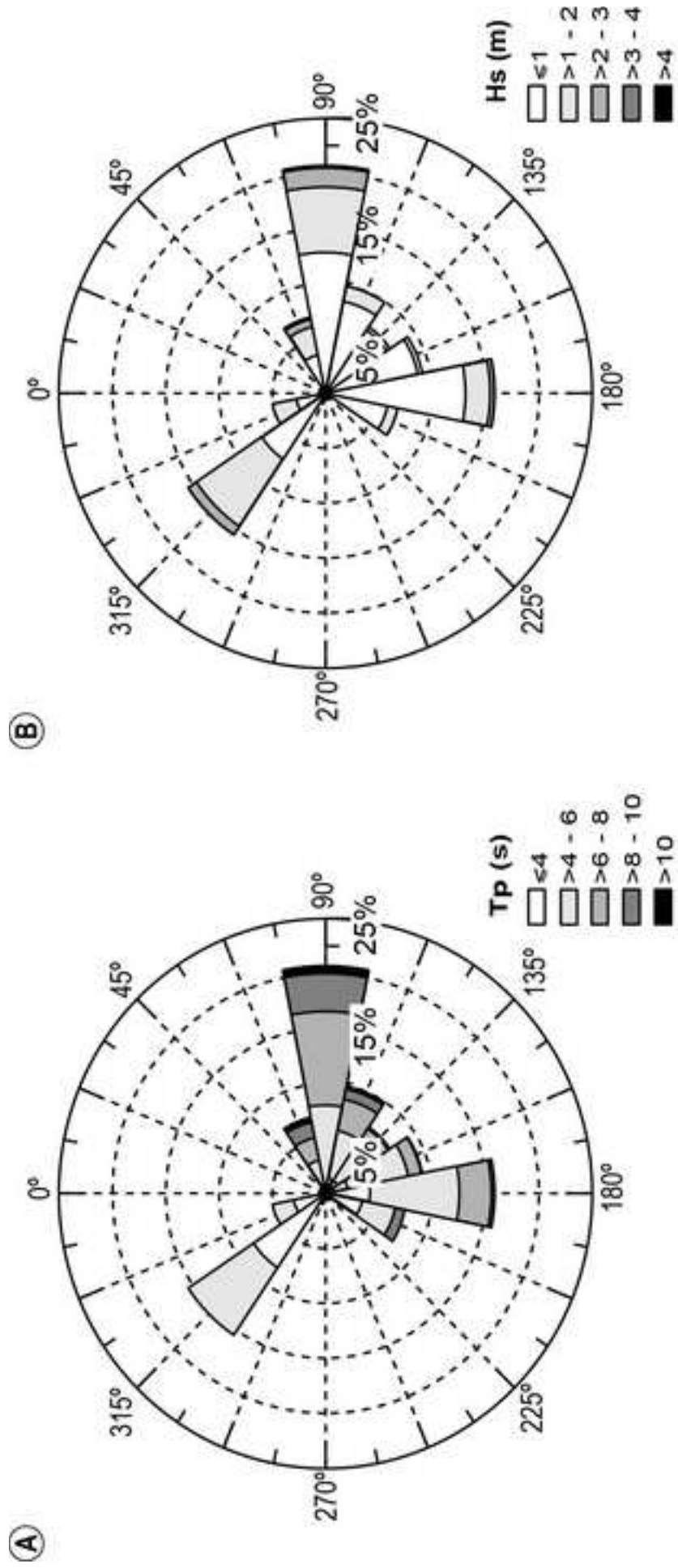
B. Across-shelf distribution of sediment transport gradient (0.063 mm grain size) during an average climatic year. $\partial \Phi / \partial z$ indicates a gradient across depth of a given parameter, which in this case refers to Φ (the transport intensity parameter).

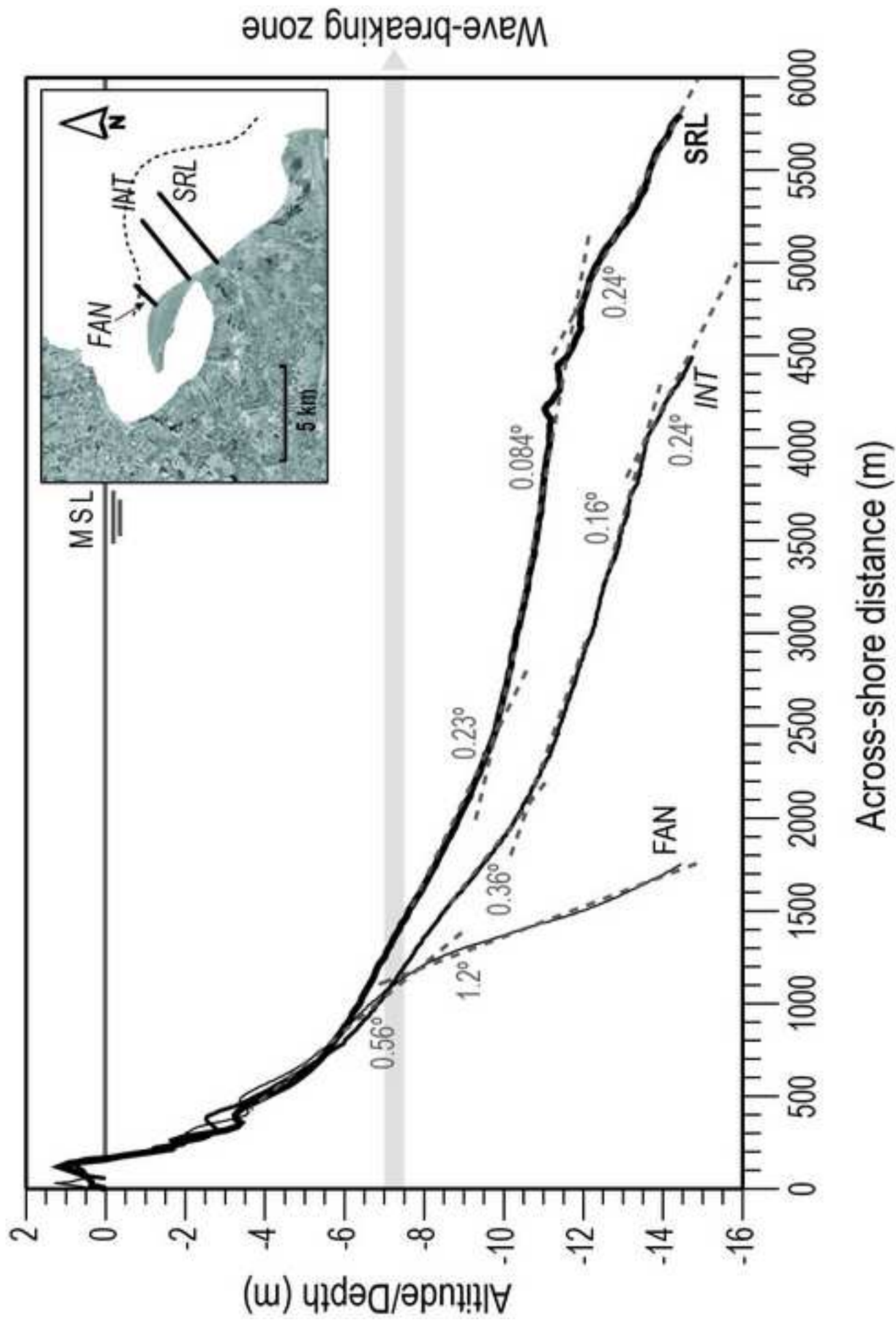
Fig. 7. Wave height amplification at the area of the relict Sol de Riu lobe during dominant coastal storm conditions ($T_p = 11$ s, ENE).

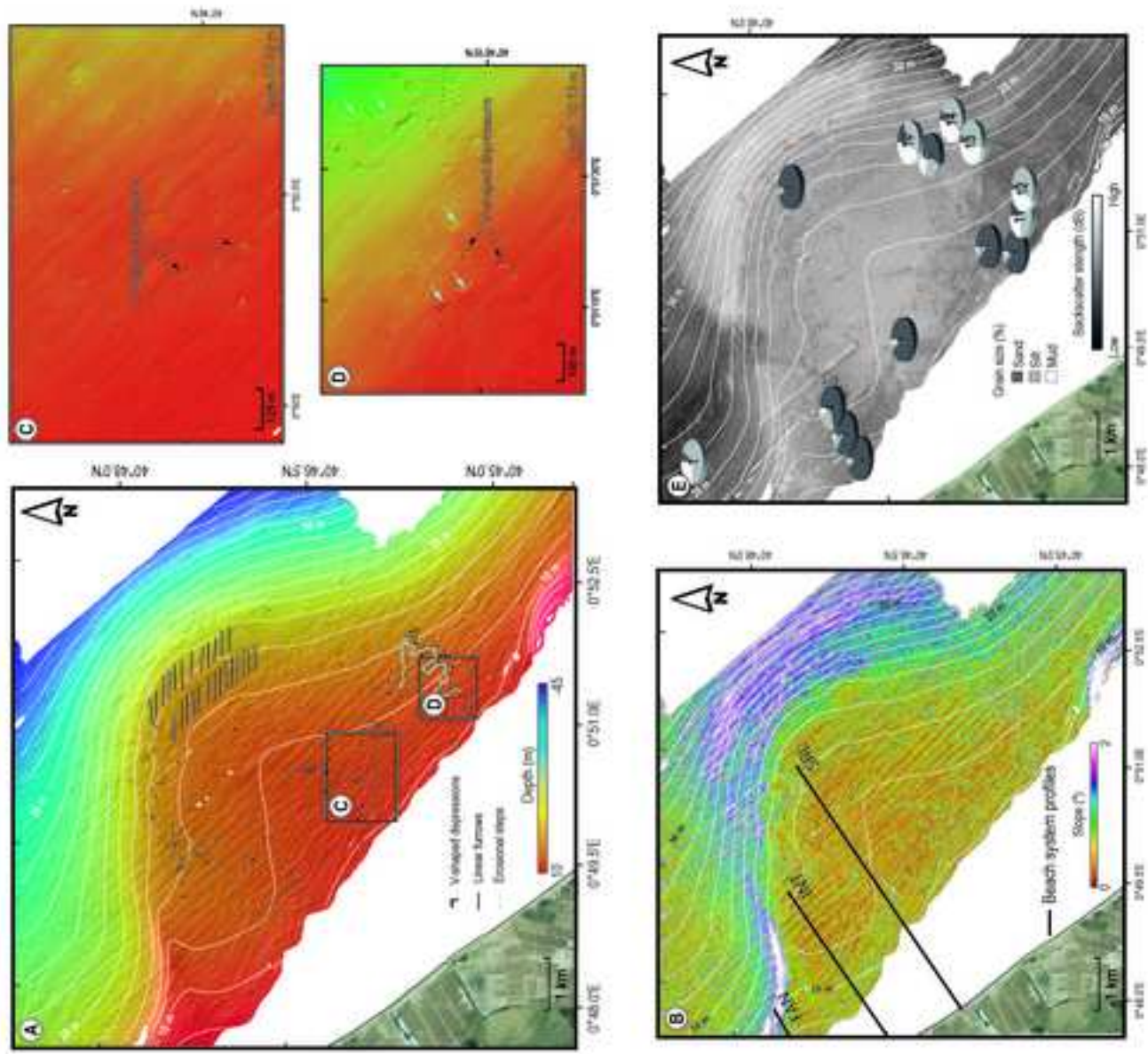
Fig. 8. Summary of the wave height amplification coefficient along the relict Sol de Riu lobe for dominant eastern waves.

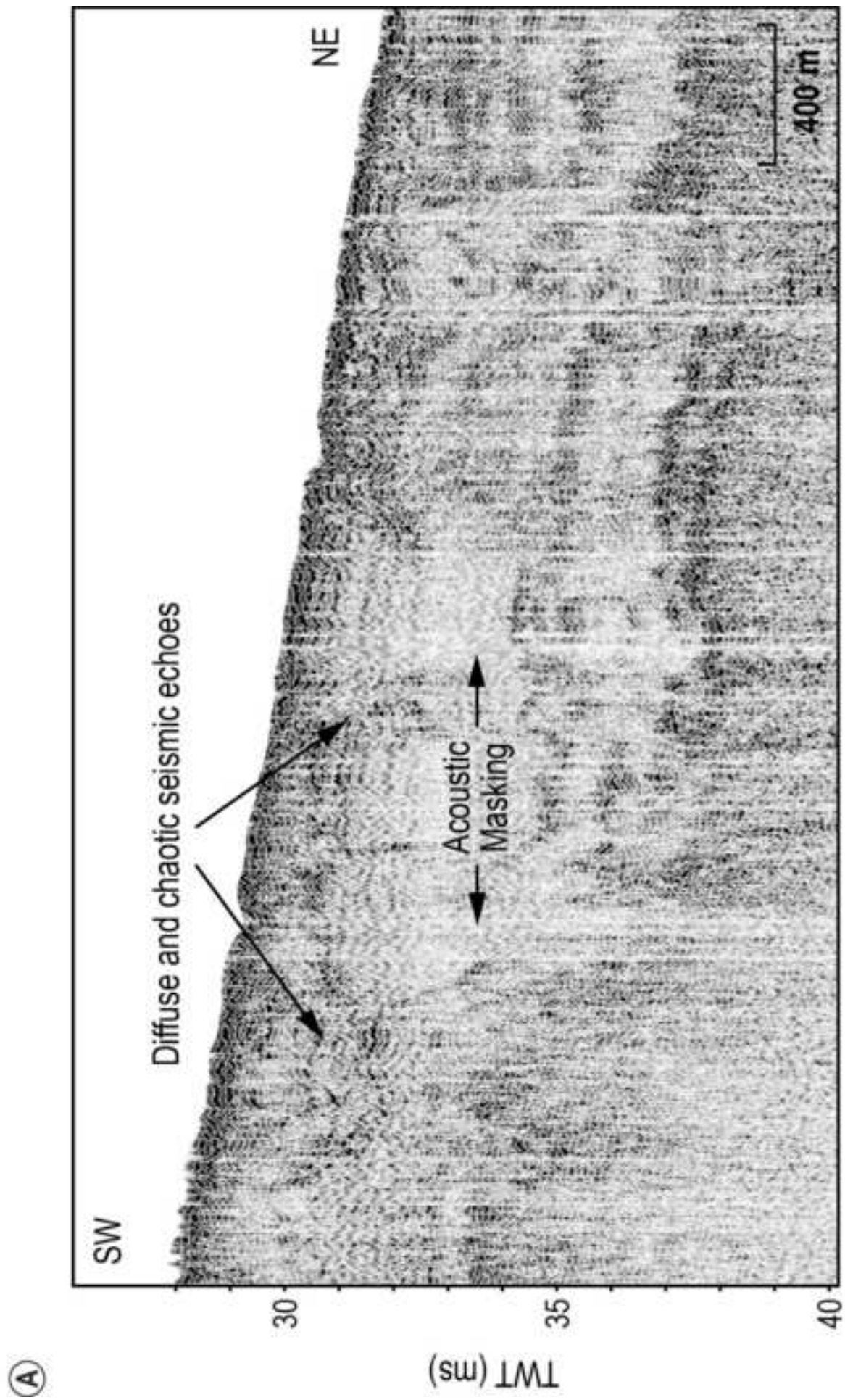
Fig. 9. Annual cumulative frequency of occurrence and contribution to overall wave energy content per wave period in the study area.

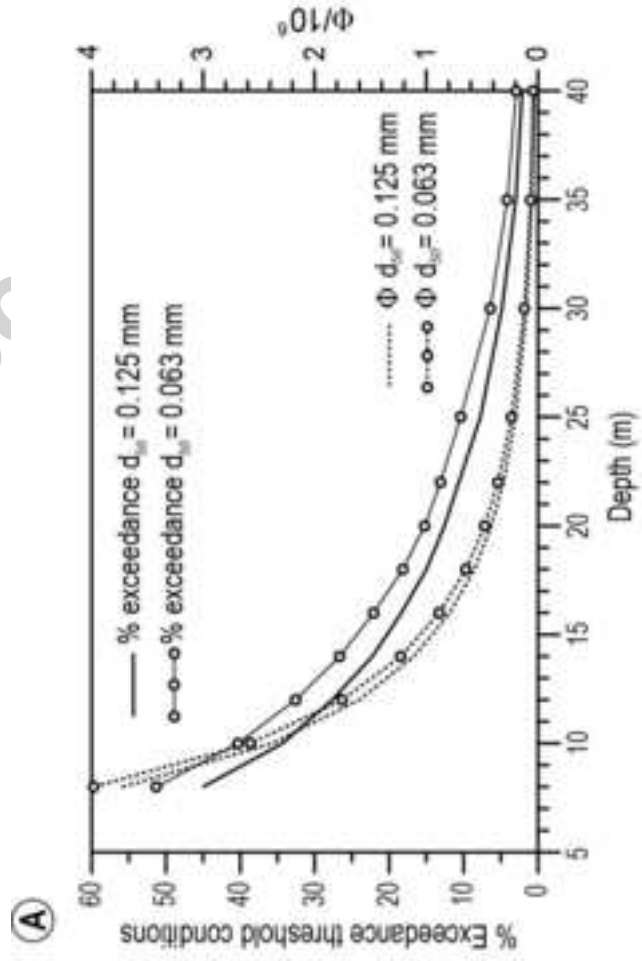
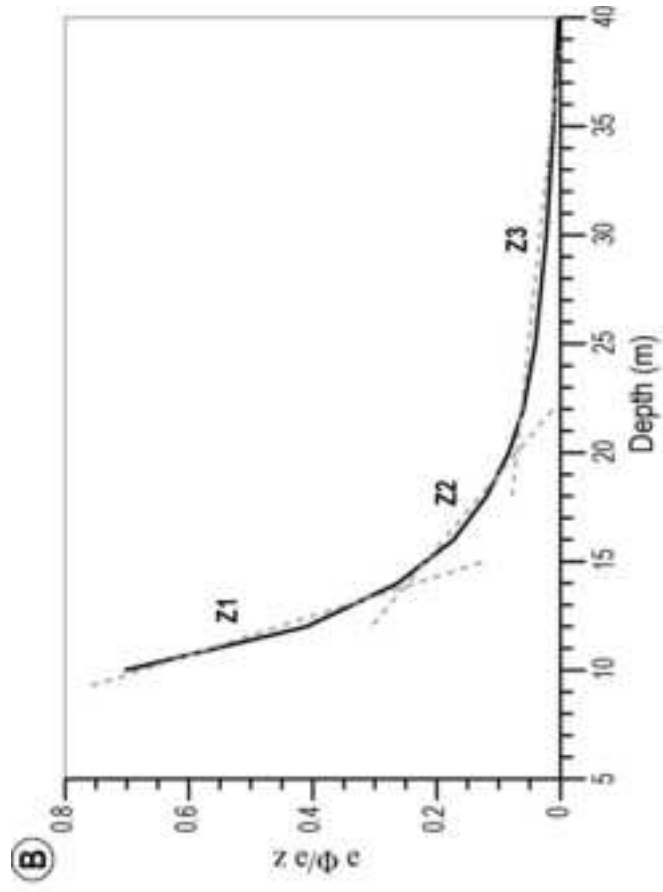
Fig. 10. Averaged shoreline displacement rates during the 1957-2007 period along La Marquesa beach landwards of Sol de Riu relict lobe. Land ortophoto courtesy of *Institut Cartogràfic de Catalunya*.











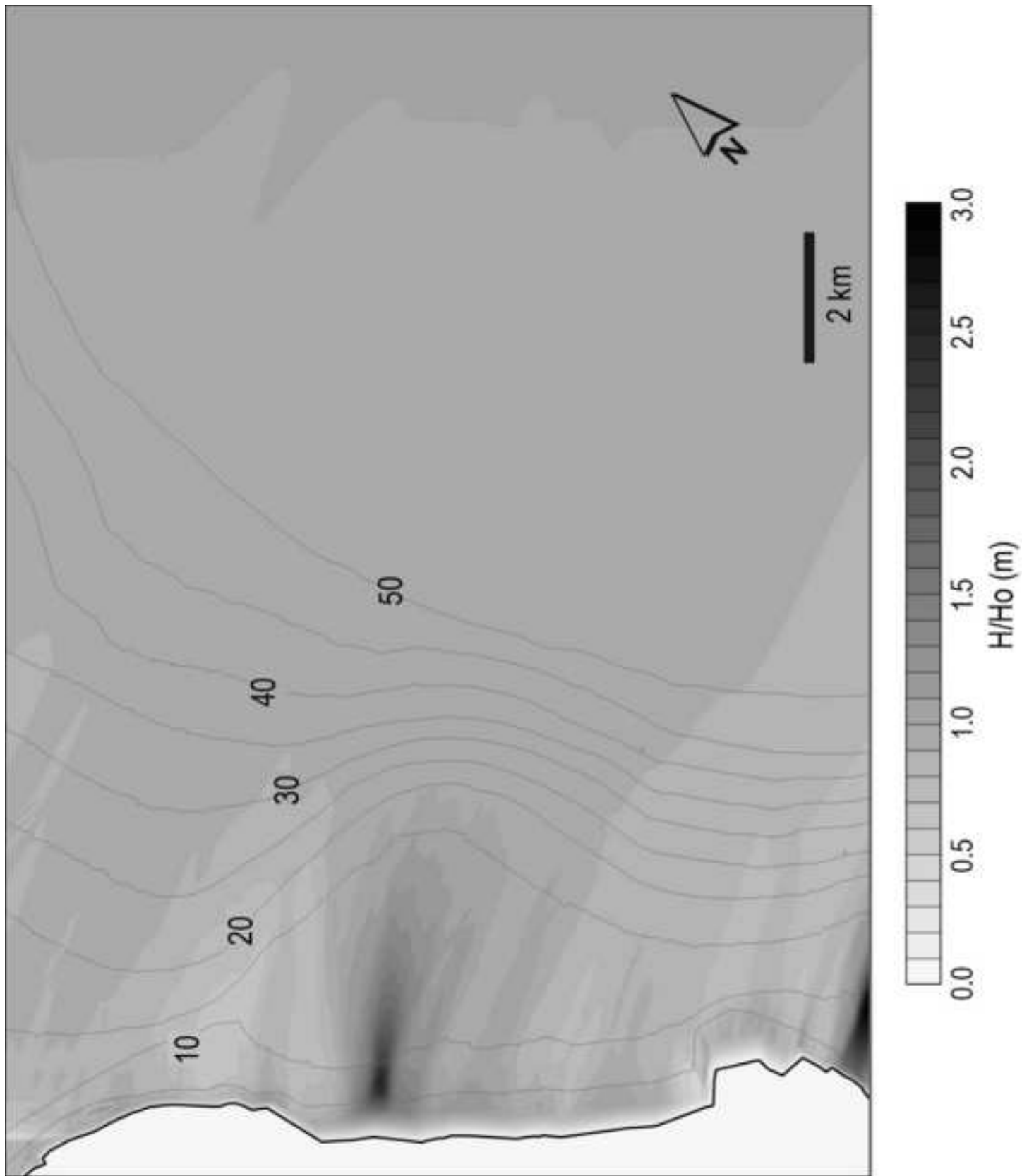


Figure_7

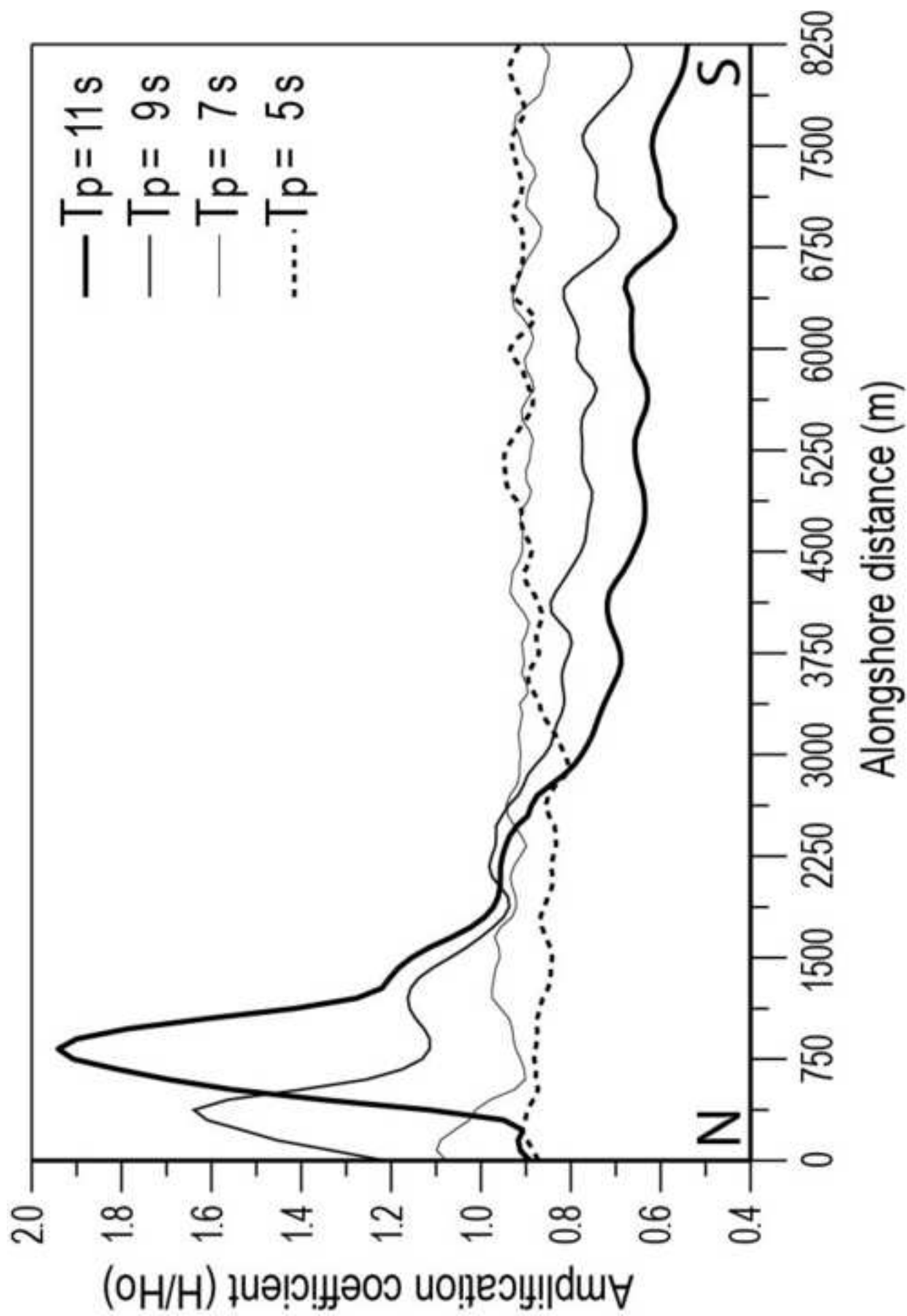


Figure_8

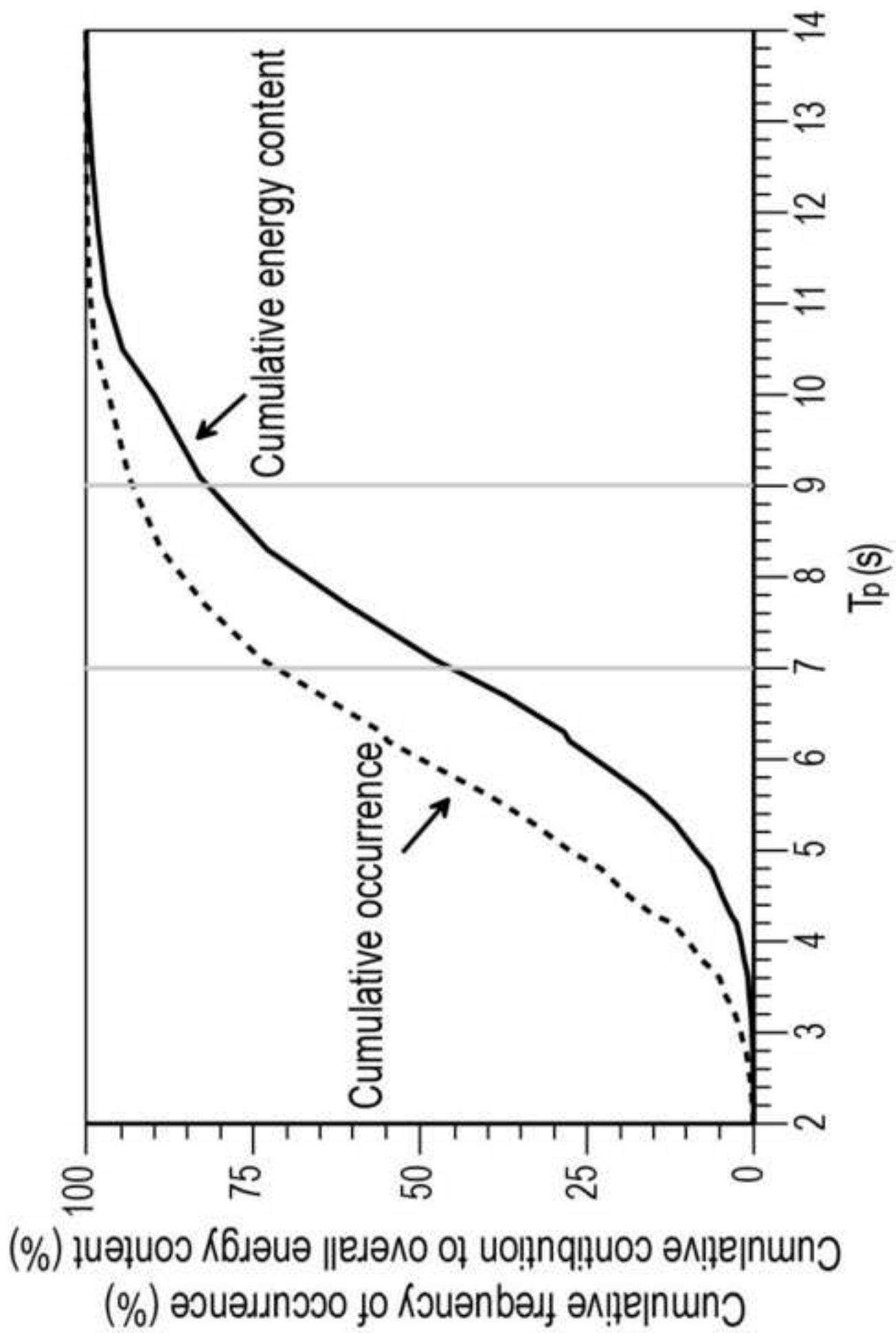


Figure_9

